

Solar photocatalytic degradation of Reactive Black 5: by-products, bio-toxicity, and kinetic study

Hamidreza Nassehinia^a, Hasan Rahmani^b, Kouros Rahmani^c, Ayat Rahmani^{a,*}

^aResearch Center for Health Sciences and Technologies, Semnan University of Medical Sciences, Semnan, Iran, Tel. +989333900151; email: ayat_rahmani@yahoo.com (A. Rahmani), Tel. +982335220132; email: hamidrezanassehi@gmail.com (H. Nassehinia)

^bDepartment of Environmental Health Engineering, School of Health, Kashan University of Medical Sciences, Kashan, Iran, email: hs.rahmani@yahoo.com (H. Rahmani)

^cDepartment of Environmental Health Engineering, Mamasani Higher Education Complex for Health, Shiraz University of Medical Sciences, Shiraz, Iran, Tel./Fax: +98 7142541387; email: krahmani@yahoo.com (K. Rahmani)

Received 26 August 2019; Accepted 7 June 2020

ABSTRACT

Reactive Black 5 (RB5) dyes are a dye widely used in textile industries. The photocatalytic oxidative degradation of aqueous solutions of RB5 dye was solar photo catalytically treated by employing the pumice modified with zinc oxide (ZnO) and nano zero-valent iron (nZVI) advanced oxidation systems in a batch reactor. The effects of samples pH (3–11), kinetic reaction, total organic carbon (TOC), and chemical oxygen demand (COD) removal, by-products, and bio-toxicity were evaluated. Characterization of the pumice, ZnO, and nZVI samples were performed by scanning electron microscopy, X-ray diffraction, X-ray fluorescence, UV-vis spectrophotometer, and Brunauer–Emmett–Teller measurements. The highest photocatalytic activity for the degradation of RB5 was obtained for the ZnO and nZVI, 99% and 90% efficiency in 120 min, respectively. The results indicate that with increasing pH (3–9) increased the rate of RB5 degradation. The gas chromatography-mass spectrometry analyses results indicate that degradation of RB5, first the ring structure is opened, and then by subsequent reactions with hydroxyl radical (OH[•]), these substances become more stable turning to mineral materials. These results show that the photocatalytic with solar light has high efficiency in RB5 removal and as well as the effluent mineralization (TOC = 90% and COD = 81%) has low toxicity in the environment.

Keywords: Photocatalytic degradation; Solar energy; Pumice; RB5 dye; ZnO; nZVI

1. Introduction

Reactive Black 5 (RB5) was one of the oldest reactive dyes and was consumed very heavily in textile dyeing [1]. Organic dyes are among the most important groups of wastewater contaminants, introduced into it through various industries including the textile industry [2]. Today, around 100,000 types of dye [3], with over 7×10^5 tons are

produced for different uses including in textile, paper, and leather production [4]. Over 280,000 tons of the total global production of dyes annually enter directly into wastewater [5]. Advanced oxidation processes (AOPs) were alternate ways for the removal of forms of refractory compounds, mainly due to the formation of HO[•] [6–8]. AOPs are a group of processes that are predicated on the generation of hydroxyl radicals. These radicals are highly reactive,

* Corresponding author.

leading to the total mineralization of most of the organic pollutants. Nanocrystalline materials mediated semiconducting photocatalysis are expeditiously becoming an efficient AOP, in which semiconductor material absorbs greater energy than its bandgap the energy which leads to the excitation of electrons from the valence band to the conduction band, consequently engendering electrons and holes. The valence band holes react with the water molecules and hydroxide ions to form hydroxyl radicals whereas the electron reacts with oxygen molecules and form superoxide radicals. These free radicals are extremely proficient oxidizers of organic dyes that can attack organic dyes and degrade them into CO_2 and H_2O [4]. The reasons for the extensive use of ZnO for photocatalytic removal of contaminants in aqueous solutions include ultraviolet adsorption and its highest stability among advanced oxidation processes [9]. Heterogeneous photocatalysis using semiconductors such as ZnO is an attractive advanced oxidation process as it has several advantages [10]. Photo-Fenton-like process, which is based using nZVI, was used. In recent years, nZVI has been successfully used for the degradation of a wide range of organics [11–13]. Due to the lower operational cost and higher capability of iron nanoparticles in terms of reducing and stabilizing different types of pollutants, it is widely used in water and wastewater. In Fenton-like (based using nano zero-valent iron) and photo-Fenton-like process (UV/nZVI/ H_2O_2), ferrous and then ferric are formed. During a regular cycle, these ions increase the efficiency of the process [14]. The supported nanoparticle on a various support materials such as zeolite activated carbon etc. has been studied in photodegradation of organic pollutants such as dyes [15]. The results of various researches suggest that as some adsorbents mixed with nanoparticles or as a catalyst is immobilized on a support adsorbent, not only the number of optical active sites increases but also it brings about increased photocatalytic characteristics due to the closeness of adsorption sites with optical active sites [16]. Pumice stone has been tested and used in various environmental applications mainly as adsorbent, filtration media, biofilm, or catalyst support, similar to the uses of sand. Pumice is a light and very porous material formed during volcanic

eruptions [17]. Pumice is a low-cost adsorbent effective in the removal of heavy metals [18]. Moreover, it provides an increase in the adsorption capacity by providing more surface area after coating [19].

This study presents experimental results solar photocatalytic degradation of RB5 by the pumice modified with ZnO and nZVI advanced oxidation systems in a batch reactor. The kinetic reaction, total organic carbon (TOC), and chemical oxygen demand (COD) removal, by-products, and bio-toxicity were evaluated. Characterization of the pumice, ZnO and nZVI samples was performed by field emission scanning electron microscopy (FE-SEM), X-ray diffraction (XRD), X-ray fluorescence (XRF), UV-vis spectrophotometer, and Brunauer–Emmett–Teller (BET) measurements.

2. Materials and methods

2.1. Materials

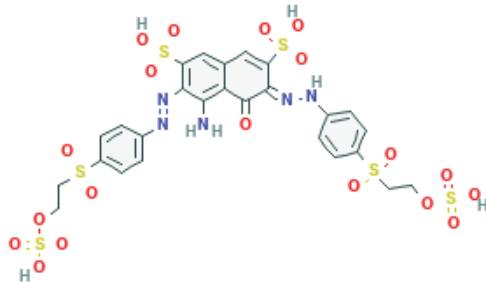
Chemicals used in the synthesis of nZVI, pumice, chlorhydric acid, sodium hydroxide, RB5 color, ferric sulfate ($\text{Fe}_2(\text{SO}_4)_3$), sodium borohydride (NaBH_4), ethanol, and starch were prepared from CMC (Germany). Molecular the structure of RB5 in non-hydrolyzed form is illustrated in Table 1.

All laboratory preparations of the study were carried out according to the regulations set in the Standard Methods. The spectrophotometer was read using a method based on the determination of the absorption of each of these concentrations of RB5 color at wavelengths 200–800 nm. The pH of the solution, which was adjusted by adding dilute aqueous solutions of NaOH or H_2SO_4 was maintained at 3, to prevent the precipitation of $\text{Fe}(\text{OH})_3$ [20]. The other chemicals such as NaOH, H_2SO_4 , and H_2O_2 (30%, w/w) (Merck) were used as such. The double-distilled water was used for the preparation of experimental solutions.

2.2. Preparation and characterization

The pumice used in this investigation was natural pumice that was obtained from the region (north-west of Iran). The chemical composition of the pumice determined by an

Table 1
Molecular structure of RB5

Molecular formula	$\text{C}_{26}\text{H}_{25}\text{N}_5\text{O}_{19}\text{S}_6$
Molecular structure	
Molecular weight	279 g/mol
Maximum wavelengths	598 nm

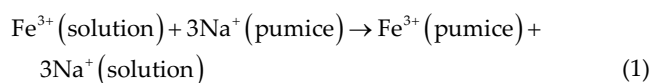
Oxford (ED2000) XRF equipment. The surface morphology and shape of samples were taken by a scanning electron microscopy (SEM) system (model: XL-30, Philips). The BET machine has been used to determine the effective surface of nanoparticles in both powdered forms and after coating conditions. In this experiment, the raw pumice and modified pumice samples were first prepared in the form before coating, and then the nanoparticles after coating were prepared to test the effective surface area.

2.2.1. pH point of zero charge

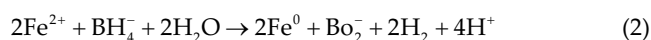
For determining pH point of zero charge (pH-Z) pumice raw and modified, the 0.01 molar solutions of sodium chloride as an electrolyte and NaOH and HCl with the purity of 0.1 molar were used as a controlling factor of pH. Pore 30 mL of the electrolyte solution in six of 50 mL and adjusts its pH to a range of 2–12 using acids and alkaline. Then add 0.5 g pumice to each airline. Was put on the shakers a speed of 120 rounds per minute for 48 h and their final pH level was read using pH-meter after infiltration. The pH-Z point of pumice was determined using the graph of the primary levels of pH. In this graph, drawing a line with a 45-degree angle with the graph, those points with the same primary and final values of pH were taken as the pH-Z [21].

2.2.2. Coating nanoparticles Fe⁰

For surface-tailored pumice with Fe₂(SO₄)₃, 50 g pumice was added a 1,000 mL of 0.075 M ferric sulfate solution. The mixtures were intermittently agitated with a shaker at 200 rpm. After 48 h the pumice was washed several times using demineralized water to decrease the electrical conductivity. Finally, the modified pumice was dried in the ambient air for 48 h [22]. After converting the pumice to its cationic form with a sodium chloride solution and adding the cationic pumice into the metal salt solution, the Na⁺ bound in the structure of the pumice was exchanged with Fe³⁺ from aqueous solution (Eq. (1)):



One gram of the pumice with 30 mL of Fe₂(SO₄)₃ solution (1 M) in the presence of nitrogen gas mixed for 3 h. Then this solution was diluted five-fold with ethanol and water solution (1:1). In the next step, 100 mL of NaBH₄ was added to this mixture at 25°C and placed on the magnetic stirrer for 30 min. After this time period, according to the Eq. (2) pumice were coated. The nZVI was separated and then washed three times with acetone at 65°C using injecting nitrogen gas stored in a desiccator [23].



2.2.3. Coating nanoparticles ZnO

The ZnO nanoparticle is purchased from the X-ray diffractometer (XRD) analysis showed an average particle

diameter of 21 nm. The purity of this nanoparticle is 99.5% and its effective surface is 51.1 m²/g. In this research, the coating method is used on the surface of pumice. First, the surface of the substrate was completely washed with distilled water. Then the pumice was contacted with NaOH with one normality. Then for making the ZnO solution, the ZnO powder with 99.5% purity was prepared and the solution with 3% ZnO was made. In the next step, the solution is placed in an ultrasonic apparatus at 50°C for 90 min to obtain a homogeneous mixture. After distributing this homogeneous suspension on the pumice surface, we place it at a normal temperature for 3–4 h. After this period of time, the amount of water remaining on the residual pumice surface was removed and the sample was placed at a normal temperature for 24 h to dry again. After this step, the pumice is placed in the furnace for 1 h and a half, and the temperature gradually increases from 50°C to 500°C to create the calcification of the nanoparticles on the substrate surface [24].

2.3. Solar experiment

All experiments were performed under natural solar radiation in Tehran–Iran that geographical location, 3 min at 25° to 39° and 47 min north latitude and 44°, 63°, 18 min east longitude 5 min which had a very good position to use solar energy. All the experiments were conducted in duplicate on twin reactors (ZnO and nZVI) under the same meteorological conditions and to ensure reproducibility of results, each sample was done three times. Tests started at 11 am and finished at 15 pm local time. Samples were taken after 5–120 min of solar exposure. The reactors were placed to the N–S and at an angle of 35° to a 15° considering region and the season and they were sampled. Solar and UV_A irradiance was measured with a global UV radiometer (295–385 nm UV and 400–1,500 nm solar, model HAGNER, Sweden) [22]. The initial temperature of all samples was about 20°C.

2.4. GC/mass analysis

In order to identify the various intermediates (formed during the dye oxidation) present in the treated dye, the samples are used in the GC/MS device. The samples in this section are tested at 15, 90, and 120 min intervals. For sample preparation 9 cc of filtered sample along with 5 cc of methanol with GC grade and 1 cc of chloroform are mixed in falcon tube made of polyethylene, and placed in a centrifuge machine with 3,500 rpm for 30 min; then, 1 cc of the solution in the separated phase was removed from the surface and injected into the GC/MS device.

2.5. Reaction kinetics

In this study, Eq. (3) was used to calculate the reaction kinetics.

$$\ln \frac{C}{C_0} = -k_t \quad (3)$$

In this equation, C₀ is the initial concentration and C is the concentration of the wastewater. *t* is the solution contact time in the reactors and *k* is the reaction speed constant.

2.6. TOC test

The TOC test was used to control the process of mineralization of the samples and to determine the ingredients of the organic matter of the wastewater. For this purpose, 10 cc of the sample was taken and after injecting 0.1 cc HCl 1 normal, the non-purgeable organic carbon (NPOC) content of the sample was measured by the TOC meter machine at 800°C furnace temperature. The model of the device was Jena-C3100 made in Germany [25]. The COD was measured by Open reflex methods [26].

3. Results and discussion

3.1. Structural analysis

XRF analysis was performed on samples to determine the mineral composition of both bare pumice and nZVI coated pumice. The obtained result from the chemical analysis of the sample is shown in Table 2. The results of the structural characterization tests showed that this mineral sample was mostly composed of pumice (over 65%) and some impurities such as clays, feldspar quartz. As can be seen from these results, Fe₂O₃ content of the nZVI coated pumice rises from 2.6% to as high as 16.9%. This result indicated that the pumice was coated successfully with nZVI, being consistent with previous characterization results. While the zinc oxide coating on the pumice has little effect on its structure, there is a good correlation between the two materials after the coating process [27].

XRD analysis confirmed the wurtzite ZnO type structures with peak broadening are shown in Fig. 1a. Further cumulative undersize distribution of precipitated ZnO particles confirmed that the particle shapes were spherical or ellipsoidal with diameters of 20 and 35 nm, respectively,

which were consistent with the crystallite size calculated by Scherrer's formula using the (100) and (002) diffraction peaks observed in XRD spectra (Fig. 1a). XRD analysis confirmed the nZVI type structures with peak broadening is illustrated in Fig. 1b. The characteristic broad peak at 2θ of 45°, 55°, 65°, and 83° indicates that the zero-valent iron is predominantly present in the sample.

The surface areas of raw pumice were 1.8 m²/g BET. After coating with the nZVI, the pumice surface area expanded 6.6 m²/g approximately 3.5 times. Furthermore, stated that the iron coating of sand enhanced the surface area from 0.85 to 2.76 m²/g [28]. Similarly reported that the surface area of synthesized kaolinite-nZVI material was 6.9 m²/g [29]. Despite this lower surface area of nZVI and ZnO compared to nZVI and ZnO alone (41–47 m²/g). In this study, the UV absorption rate by nanoparticles was investigated at a wavelength range of 200–1,000 nm by UV-vis diffuse reflectance spectroscopy (DRS). The results of this analysis show that the highest UV absorption for ZnO is at 250 nm wavelength in the UV_C wavelength range. The nanoparticle also has a maximum absorption rate at wavelengths of 320–360 nm, which are located in the UV_A wavelength range. This nanoparticle has a very low absorption at wavelengths higher than 400 nm, which is in the range of the visible light of the sun [30] (Table 3). From UV-vis spectrum of nZVI particles, it was observed that smooth and narrow absorption bands were obtained at 200 and 368.3 nm corresponding to the excitation of surface plasmon vibrations in the nZVI the solution which is characteristic of monodispersed iron nanoparticles. The nZVI in the range of wavelengths of the solar light absorption rate is about 18% (Table 3).

In Fig. 2a FE-SEM shows the surface of the pumice substrate before coating, which caused the contact of the substrate with HCl on the pumice surface to provide a suitable

Table 2
XRF results of chemical compositions for pumice

	LOI	Na ₂ O	MgO	Al ₂ O ₃	SiO ₂	P ₂ O ₅	SO ₃	K ₂ O	CaO	TiO ₂	Fe ₂ O ₃
Pumice	8.01	1.87	0.866	14.5	66.1	0.14	0.037	2.7	2.5	0.42	2.61
P-nZVI	7.91	4.2	0.89	13.8	50.7	0.15	0.041	2.71	2.3	0.43	16.9
P-ZnO	7.88	3.6	0.81	14.1	64.6	0.13	0.036	2.67	2.41	0.42	3.1

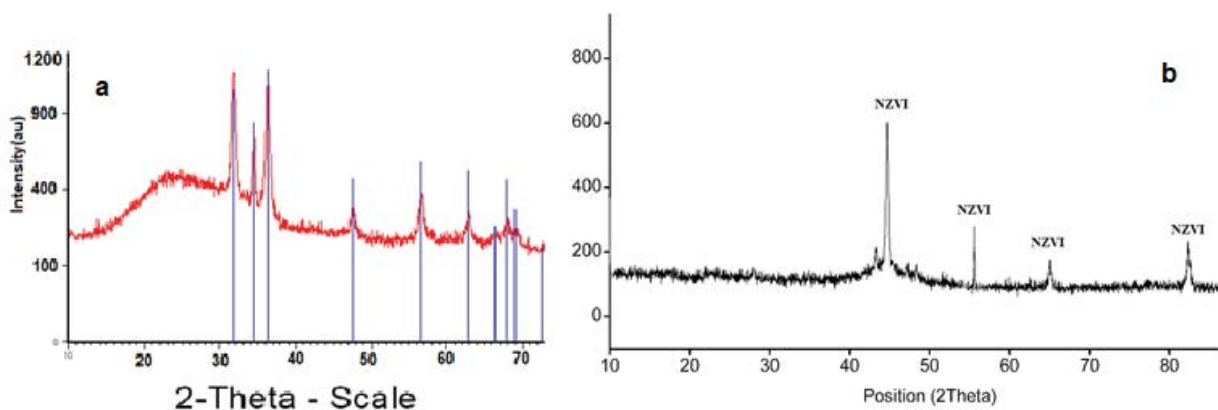


Fig. 1. XRD diffractograms for ZnO (a) and nZVI (b) after coating.

Table 3
Crystallite sizes, surface areas, band gap energies E_g and absorption wavelengths for the samples

	BET m ² /g	Cristal Size(nm)	E_g (eV)	UV absorption edge (nm)
Pumice	1.8	11.1	–	–
Pumice-nZVI	6.6	35	1.7	368.8 nm
Pumice-ZnO	7.3	18	3.01	377 nm
nZVI	41.6	31	1.7	368
ZnO	47.2	21	3.02	378 nm

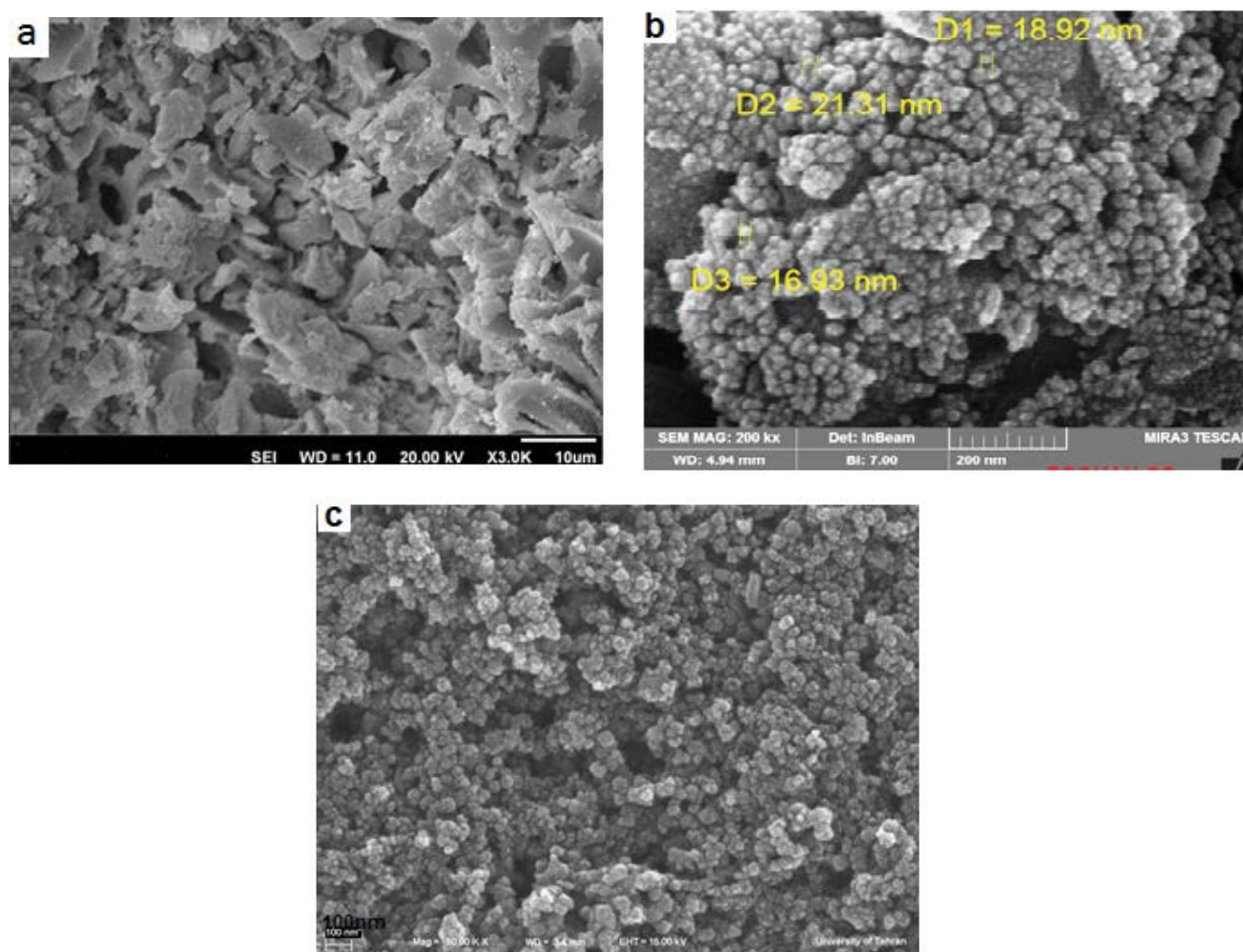


Fig. 2. FESEM surface of the pumice substrate before coating before coating (a), after coating with ZnO (b), and nZVI (c).

substrate for the nanoparticle coating and after coating with ZnO (Fig. 2b) and nZVI (Fig. 2c) that the nanoparticle is uniformly distributed over the entire surface.

3.2. UV-visible analysis

Photodegradation before and during treatment was studied using UV-visible analysis (200–800 nm). The spectrum of RB5 in the visible and UV region exhibits the main band with a maximum wavelength (λ_{max}) at 598 and 312 nm in visible and UV regions, respectively, as shown

in Fig. 3. It has been observed from Fig. 3 that maximum wavelength peaks are not shifting after degradation of dye till 90 min.

3.3. Solar light

The essays were carried out on sunny days without cloud cover. Fig. 4 shows the peak sun hours of 11.30 to 14.30, so tests were done at the same time. The maximum solar light and UV radiations were 800 and 33.4 W/m², respectively (Fig. 4).

3.4. Dye degradation

Fig. 5 shows the photocatalytic degradation of dye with reactors ZnO and nZVI with solar light. It is noticed that the highest rate of degradation in ZnO is 99% after 120 min. The combined action of nZVI caused 89.3% degradation in 120 min. For solar alone, it was observed that the dye degradation about 18% in 120 min. The most important factor in the degradation of RB₅ is the presence of free radicals of OH resulting from the photocatalytic process. As shown in Fig. 5, the ZnO nanoparticles absorption is at 321 nm in the wavelength of the UV_A of the solar, in conclusion, it can be said that the ZnO is capable of producing more free radicals resulting in higher efficiency in RB₅ removal.

Comparing two solar reactors, the ZnO has higher efficiency than the nZVI, which. The reason for this difference is nZVI in the range of wavelengths of solar light absorption rate is about 18%. However, the ZnO at the wavelength

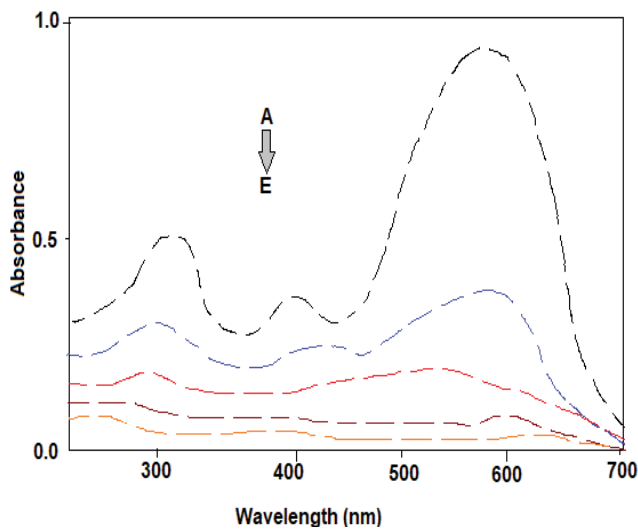


Fig. 3. UV-visible absorption spectra of RB₅ solution during photocatalytic degradation process, pumice-ZnO. Experimental conditions: RB₅ = 50mg/L, pH = 7 ± 0.1, reaction time = 120min, A = 0 min, B = 30 min, C = 60 min, D = 90 min, and E = 120 min.

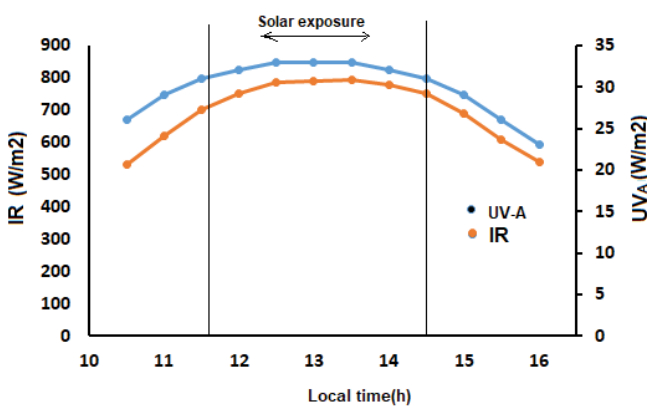


Fig. 4. Graphic representations of the values of solar UV and solar irradiance radiations registered during the degradation.

range of 300–390 has a light absorption of about 85% and can be said to have higher photocatalytic activity than nZVI [23]. As shown in previous studies, the increase in the intensity of light radiation, especially at wavelengths of 300–350 nm, grows the efficiency of the photocatalytic process, and the production of free radicals that are effective in removing RB₅ [31].

3.5. Kinetic reaction of RB₅

Photolysis in solar light and photocatalytic processes are two mechanisms that contributed to the degradation of RB₅. The Fig. 6 shows the kinetic reaction of RB₅ at a time of 5 min it can be seen that the kinetic reaction of photolysis in RB₅ the solution, which is contacted with solar light is 0.08 at 120 min. The kinetic reactions in the photocatalytic process in ZnO and nZVI are 1.21, 1.09, respectively, at 30 min. Overall, the reason for increasing the reaction rate in ZnO/solar light is due to the production of higher OH radicals than other reactors. Generally, the rate of dye degradation is higher in the photocatalytic process in the first 30 min of contact, and the photolysis process by the solar at a slower rate, and occurs uniformly over 120 min. It was reported that ZnO absorbs a large fraction of the solar spectrum. But ZnO has the disadvantage of undergoing

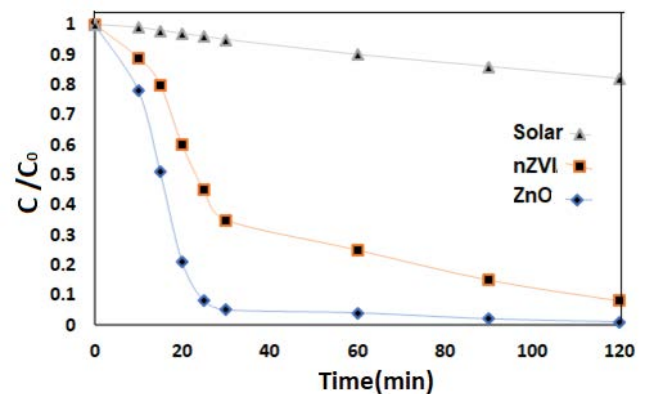


Fig. 5. Effect of solar light, ZnO, and nZVI on photocatalytic degradation of RB₅.

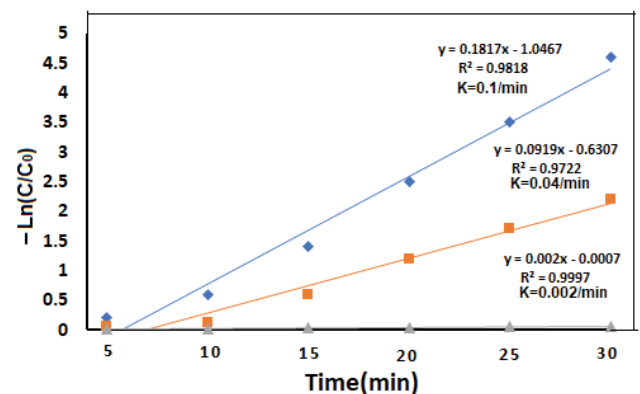


Fig. 6. Reaction kinetics of RB₅ in solar light, ZnO, and nZVI.

photo corrosion. Fe⁰ absorbs sunlight more than ZnO or TiO₂ but it has less photocatalytic activity [31].

3.6. Adsorption tests

The adsorption equilibrium time of RB5 was determined through kinetic tests performed with raw pumice and pumice modified with nZVI and ZnO. Kinetic test results showed that RB5 can be removed with raw pumice, nZVI and ZnO is 11, 18, and 9 presents, respectively, at 120 min (Table 4). The maximum absorption capacity for synthetic samples of the raw pumice were in 0.7 mg/g and for the nZVI was in 1.1 mg/g, while maximum absorption capacity of the ZnO was in 0.6 mg/g and the correlation coefficient (R^2), the Langmuir model is much better in the description of adsorption isotherm data with a higher R^2 than model Freundlich [30].

3.7. Effect of the solution pH

The effect of pH on the heterogeneous photocatalytic oxidation of hydrolyzed RB5 has been examined with ZnO at pH 3–11 and the obtained results are presented in Fig. 7. To determine the effect of pH, specify the optimal pH, and understand the effect of pH-Z in removal efficiency, in this study, RB5 dye solution with a concentration of 50 mg/L was prepared and the removal efficiency was investigated. The results of this step indicate that in the process of photocatalytic oxidation, with a rise in pH 3–9, the performance rate of RB5 degradation has increased. Assuming that the photocatalytic degradation proceeds mainly via OH[•] attack at higher pH-values, and via valence band hole ($h\nu_i^+$) oxidation at acidic and neutral pH, it is expected that degradation is favored at alkali pH, where the photocatalyst surface is highly hydroxylated. An abrupt acceleration in degradation kinetics at pH = 7–9 was also observed for the oxidation of spent reactive dye-bath liquors at different pH-values in previous work [32].

On the other hand, qualified for the color structure as well as the pumice structure and its pH-Z. As noted, before, pH-Z of unprocessed and that of modified pumice will equal 7.3 and 7.11, respectively. Analyses indicate that in pHs upper than pH-Z, active groups decay in the P-ZnO surface and thus increase in the character of these groups. Under this condition, the organic groups decomposed in the pumice surface increase the quickness of the photocatalytic oxidation reaction. The electron donating in these acidic acting groups transfers electrons to OH and increase the progress in the speed of reaction and radicalization of OH in the pumice surface. Finally, this electron

transferring makes OH anions and contributes to a radical cycle. However, with the reduction of pH of the number of sites with the positive charge on the surface of nanoparticles and the adsorbent surface increases and an electrostatic attraction develops between the site with a positive charge on the surface of nanoparticles and the molecules of reactive red 198 dye with a negative charge. With the further absorption of dye molecules, removal in turn increases. Some works of literature attribute the color degradation in the acidic conditions of the active non-hydroxyl radical in the catalyzer surface [33].

It seems that as the pH increases (9–11) The removal efficiency is reduced, that due to ionization of functional groups such as hydroxyl that it can reduce the number of hydrogen radicals, negative charge is developed across the surface of nanoparticles whereby an electrostatic repulsion is developed between the surface of the nanoparticles with a negative charge and the molecules of RB5 dye with a negative charge [34].

3.8. Effect of the photocatalytic oxidation on the degradation of COD and TOC

The results of the COD and TOC degradation efficiency of RB5 at optimized conditions with P-ZnO have been determined in Fig. 8. The amount of the COD degradation of RB5 in 15 min 14% reaching 70% in 90 min and reaching 82% at the end of the 120 min and the TOC degradation efficiency started from 12% in 5 min, reaching 83% in 90 min and reaching 91% at the end of the 120 min. The RB5 dye under optimized conditions shows high degradation efficiency and is almost completely degraded after 120 min. But COD and TOC removal are slow concerning

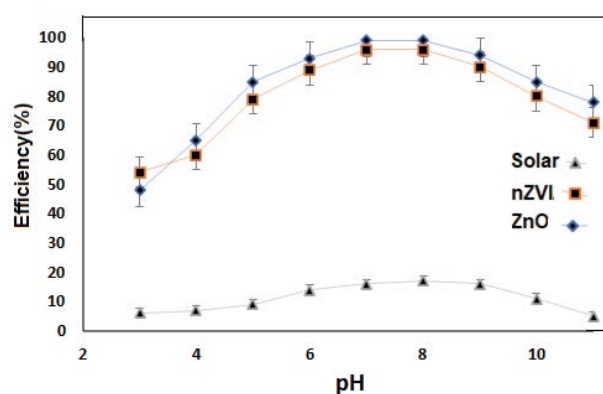
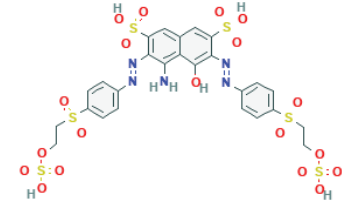
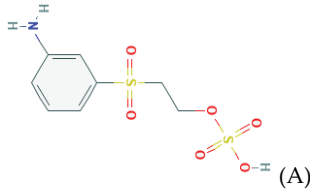
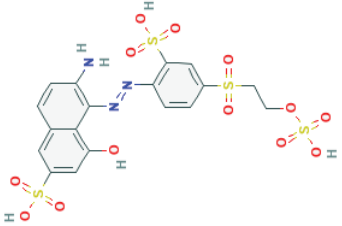
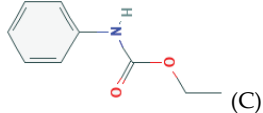
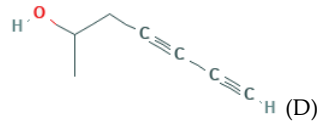
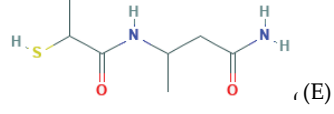
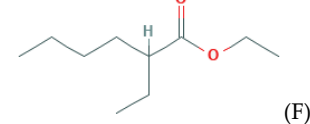
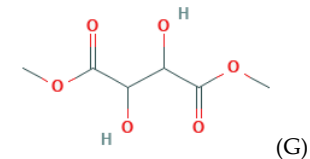
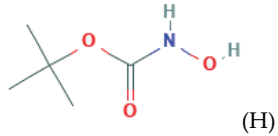
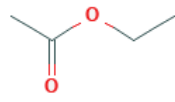


Fig. 7. Effect of pH on removal efficiency RB5 for ZnO.

Table 4
Langmuir and Freundlich coefficients for adsorption RB₅

	Langmuir model			Freundlich model		
	b	q_{\max}	R^2	K_F	n	R^2
Pumic	0.09	0.7	0.989	0.76	4.7	0.931
Pumic-ZNO	0.07	0.6	0.997	0.7	4.5	0.911
Pumic-nZVI	0.11	1.1	0.9551	0.87	7.1	0.9276

Table 5
Molecular structure compounds that were possibly created by the degradation of RB5 in GC-MAS test

Time (min)	Molecular formula	Molecular formula	Molecular structure
0	$C_{26}H_{25}N_5O_{19}S_6$	RB5	
	$C_8H_{11}NO_6S_2$	2-(3 aminophenyl)sulfonylethyl hydrogen sulfate	
15	$C_{18}H_{17}N_3O_{13}S_4$	6-amino-4-hydroxy-5-[[2-sulfo-4-(2-sulfoxyethylsulfonyl) phenyl] diazenyl] naphthalene-2-sulfonic acid	
	$C_9H_{11}NO_2$	N-phenylurethane	
	C_7H_8O	Hepta-4,6-diyne-2-O ₁	
90	$C_7H_{14}N_2O_2S$	3-(2-Sulfanylpropanoylamino) butanamide	
	$C_{10}H_{20}O_2$	Ethyl 2-ethylcaproate	
	$C_6H_{10}O_6$	Butanedioic acid 2,3-dihydroxy-dimethyl Ester	
120	$C_5H_{11}NO_3$	Tert-butyl N-hydroxycarbamate	
	$C_4H_8O_2$	Ethyl ethanoate	
		CO_2, SO_4, NO_4	

degradation efficiency. This will be due to the formation of intermediates and later on, these intermediates have been degraded, and RB5 mineralized after 120 min.

3.9. By-products and intermediates

The GC-MS analysis was carried out to recognize potentially available organic/aromatic compounds/intermediates formed during the photocatalytic degradation of RB5. In the samples of the reactors were extracted at times 15, 90, and 120 min. Compounds that were possibly created by the degradation of RB5 and indicated by the GC-MS test in Fig. 9 (GC-MS) and Table 5 (molecular structure) and from (A) to (I) were numbered, respectively.

3.9.1. By-products after 15 min exposure

OH^{\bullet} , free radicals created in the photocatalytic process can cause breaking structures between the C–H, C–N, C–S, O–C bonds. As shown in Table 5 and Fig. 9, in the first 15 min of the reaction, after breaking down the contaminant's structure, materials such as (A) 2-(3 aminophenyl) sulfonyl ethyl hydrogen sulfate, (B) 6-amino-4-hydroxy-5-[[2-sulfo-4-(2-sulfoxyethylsulfonyl)phenyl]diazonyl] naphthalene-2-sulfonic acid, (C) N-phenylurethane which still preserved the ring structure [30].

3.9.2. By-products after 90 and 120 min exposure

After 90 min, the materials in contact with free radicals are broken down and form a simpler material that contains mostly of (D) hepta-4,6-diyne-2-ol, (E) 3-(2-sulfanylpropanoylamino) butanamide, (F) ethyl 2-ethyl caproate after 120 min exposure (G) butanedioic acid 2,3-dihydroxydimethyl ester, (H) tert-butyl N-hydroxycarbamate, and (I) ethyl ethanoate whose structure is shown in Fig. 9 and Table 5. Subsequently, the ring structure of these compounds is further converted to simpler materials in contact with OH^{\bullet} . They had interpreted the reaction mechanism in relation to the photogenerated OH^{\bullet} radicals and settled that the two compounds are completely converted to by-products that undergo further degradation with the breaking of the aromatic compounds. Finally, these substances become

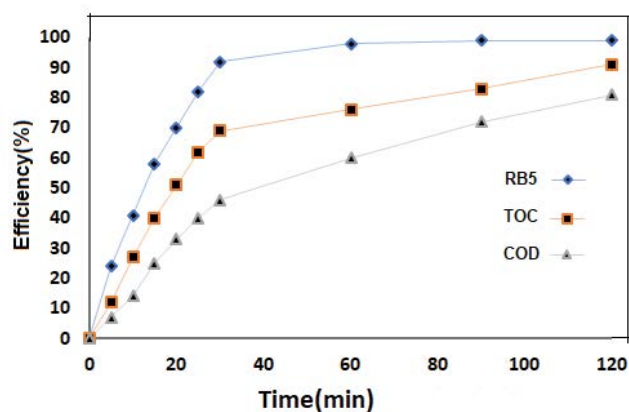


Fig. 8. Rate of the COD and TOC degradation of RB5 for P-nZVI.

more stable turning to mineral materials containing sulfate nitrate, and ammoniac compound after oxidation [30].

3.10. Bio-toxicity test

Bio-toxicity assessment with *Vibrio fischeri* was investigated and the results obtained are shown in Fig. 10. The *V. fischeri* mortality was recorded to be 24%, 41.1%, and 91.4% at a dye concentration of 50, 100–400 mg/L, while at an initial dye the concentration of 600 or above, complete mortality of *Vibrio Fischer* was noted. After treatment, the mortality rate was significantly reduced and found to be in the range of 4%–30%. The results thus evidencing the less toxic nature of the degraded metabolites compared to the toxic RB5. Lade et al. [35] observed the complete death of *D Magna* when exposed to untreated azo dyes, while biodegraded samples showed greater crustacean survival. The results clearly highlight the possible implication of the photocatalytic system for the detoxification and degradation of textile reactive dyes [35–38].

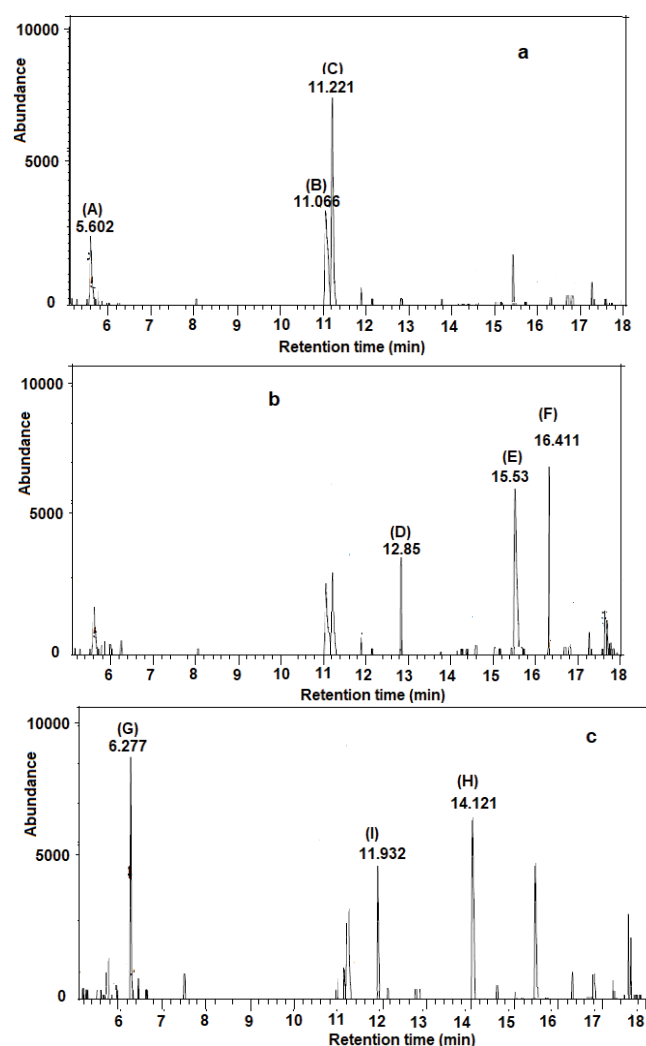


Fig. 9. GC-MS chromatogram of the degradation of RB5, after 15 min exposure (a), after 90 min exposure (b), and after 120 min exposure (c).

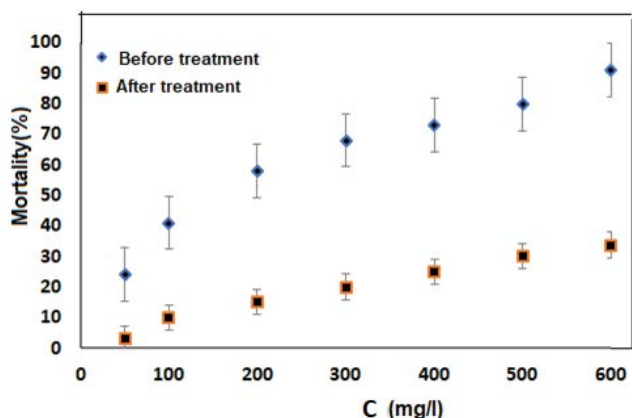


Fig. 10. Acute bio-toxicity evaluations using *Vibrio fischeri* after 48 h of incubation at different dye concentrations.

4. Conclusions

The results indicate that the highest photocatalytic activity for the degradation of RB5 was obtained for the ZnO and nZVI, 99% and 90% efficiency in 120 min, respectively. The results indicate that with increasing pH 3–9 increased the rate of RB5 degradation. The GC-MS analyses results indicate that degradation of RB5, first the ring structure is opened and then by subsequent reactions with OH radicals, these substances become more stable turning to mineral materials. These results show that the photocatalytic with solar light has high efficiency in RB5 removal and as well as the effluent mineralization TOC = 90% and COD = 81% has low toxicity to the environment.

References

- I. Ashlan, B. Akmehtmet, Degradation of commercial reactive dyestuffs by heterogenous and homogenous advanced oxidation process: a comparative study, *Dyes Pigm.*, 43 (1999) 95–108.
- A. Aguedach, S. Brosillon, J. Morvan, E.K. Lhadi, Photocatalytic degradation of azo-dyes reactive black 5 and reactive yellow 145 in water over a newly deposited titanium dioxide, *Appl. Catal., B*, 57 (2005) 55–62.
- M. Ehrampoosh, G. Moussavi, M. Ghaneian, S. Rahimi, M. Ahmadian, Removal of methylene blue dye from textile simulated sample using tubular reactor and TiO₂/UV-C photocatalytic process, *J. Environ. Health Sci.*, 8 (2011) 34–40.
- N.M. Mahmoodi, M. Arami, N.Y. Limaee, Photocatalytic degradation of triazinic ring-containing azo dye (Reactive Red 198) by using immobilized TiO₂ photoreactor: bench scale study, *J. Hazard. Mater.*, 133 (2006) 113–118.
- A. Rahmani, J. Nouri, S. Kamal Ghadiri, A. Mahvi, M.R. Zare, Adsorption of fluoride from water by Al³⁺ and Fe³⁺ pretreated natural Iranian zeolites, *Int. J. Environ. Sci.*, 4 (2010) 607–614.
- S. Nachiappan, K. Muthukumar, Intensification of textile effluent chemical oxygen demand reduction by innovative hybrid methods, *Chem. Eng. J.*, 163 (2010) 344–354.
- H. Rahmania, A. Rahmanic, M. Yousefid, K. Rahmanid, Degradation of sulfamethoxazole antibacterial by sono-Fenton process using nano-zero valent iron: influence factors, kinetic and toxicity bioassay, *Desal. Water Treat.*, 150 (2019) 220–227.
- M. Gholami, K. Rahmani, A. Rahmani, H. Rahmani, A. Esrafil, Oxidative degradation of clindamycin in aqueous solution using nanoscale zero-valent iron/H₂O₂/US, *Desal. Water Treat.*, 57 (2016) 13878–13886.
- M. Fazlzadeh, A. Rahmani, H.R. Nassehinia, H. Rahmani, K. Rahmani, Degradation of sulfathiazole antibiotics in aqueous solutions by using zero valent iron nanoparticles and hydrogen peroxide, *Koomesh*, 18 (2016) 350–356.
- M. Hassaan, M.E. Katory, R.M. Ali, A.E. Nemr, Photocatalytic degradation of reactive black 5 using photo-Fenton and ZnO nanoparticles under UV irradiation, *Egypt. J. Chem.*, 119 (2020) 17–18.
- M. Karimaei, B. Shokri, M.R. Khani, K. Yaghmaeian, A. Mesdaghinia, R. Nabizadeh, A.H. Mahvi, S. Nazmara, Comparative investigation of argon and argon/oxygen plasma performance for Perchloroethylene (PCE) removal from aqueous solution: optimization and kinetic study, *J. Environ. Health Sci.*, 16 (2018) 277–287.
- H. Chen, Y. Cao, E. Wei, T. Gong, Q. Xian, Facile synthesis of graphene nano zero-valent iron composites and their efficient removal of trichloronitromethane from drinking water, *Chemosphere*, 146 (2016) 32–39.
- J. Zhang, Q. Liu, Y. Ding, Y. Bei, 3-aminopropyltriethoxysilane functionalized nanoscale zero-valent iron for the removal of dyes from aqueous solution, *Pol. J. Chem. Technol.*, 13 (2011) 35–39.
- C.-H. Weng, Y.-T. Lin, C.-K. Chang, N. Liu, Decolourization of direct blue 15 by Fenton/ultrasonic process using a zero-valent iron aggregate catalyst, *Ultrason. Sonochem.*, 20 (2013) 970–977.
- M. Karimaei, R. Nabizadeh, B. Shokri, M.R. Khani, K. Yaghmaeian, A. Mesdaghinia, A. Mahvi, S. Nazmara, Dielectric barrier discharge plasma as excellent method for Perchloroethylene removal from aqueous environments: degradation kinetic and parameters modeling, *J. Mol. Liq.*, 248 (2017) 177–183.
- M. Rismanchian, S. Barakat, N. Khoshzat, R. Keshavarzi, M. Shakerian, Investigation of TiO₂/zeolite photocatalytic activity for Safranin dye removal of aqueous solution, *Int. J. Environ. Health Eng.*, 4 (2015) 4–12, doi: 10.4103/2277-9183.153989.
- M. Kitis, S. Kaplan, E. Karakaya, N. Yigit, G. Civelekoglu, Adsorption of natural organic matter from waters by iron coated pumice, *Chemosphere*, 66 (2007) 130–138.
- T. Liu, Z.-L. Wang, Y. Sun, Manipulating the morphology of nanoscale zero-valent iron on pumice for removal of heavy metals from wastewater, *Chem. Eng. J.*, 263 (2015) 55–61.
- M. Yavuz, F. Gode, E. Pehlivan, S. Ozmert, Y.C. Sharma, An economic removal of Cu²⁺ and Cr³⁺ on the new adsorbents: pumice and polyacrylonitrile/pumice composite, *Chem. Eng. J.*, 137 (2008) 453–461.
- B. Xu, F. Wu, X. Zhao, H. Liao, Benzotriazole removal from water by Zn–Al–O binary metal oxide adsorbent: behavior, kinetics and mechanism, *J. Hazard. Mater.*, 184 (2010) 147–155.
- S. Saravanan, T. Sivasankar, Ultrasound-assisted Fenton's treatment of Reactive Black 5 dye: effect of system parameters, kinetics and mechanism, *Desal. Water Treat.*, 56 (2015) 492–501.
- A. Yazdanbakhsh, A. Rahmani, M. Massoudinejad, M. Jafari, M. Dashtdar, Accelerating the solar disinfection process of water using modified compound parabolic concentrators (CPCs) mirror, *Desal. Water Treat.*, 57 (2016) 23719–23727.
- M. Ahmadi, K. Rahmani, A. Rahmani, H. Rahmani, Removal of benzotriazole by photo-Fenton like process using nano zero-valent iron: response surface methodology with a Box–Behnken design, *Pol. J. Chem. Technol.*, 19 (2017) 104–112.
- M. Farzadkia, K. Rahmani, M. Gholami, A. Esrafil, A. Rahmani, H. Rahmani, Investigation of photocatalytic degradation of clindamycin antibiotic by using nano-ZnO catalysts, *Korean J. Chem. Eng.*, 31 (2014) 2014–2019.
- A.V. Emeline, V.N. Kuznetsov, V.K. Rybchuk, N. Serpone, Visible-light-active titania photocatalysts: the case of N-doped s – properties and some fundamental issues, *Int. J. Photoenergy*, 2008 (2008) 1–20, doi: 10.1155/2008/258394.
- S. Sato, R. Nakamura, S. Abe, Visible-light sensitization of TiO₂ photocatalysts by wet-method N doping, *Appl. Catal., A*, 284 (2005) 131–137.

- [27] B.I. Harman, M. Genisoglu, Synthesis and characterization of pumice-supported nZVI for removal of copper from waters, *Adv. Mater. Sci. Eng.*, 2016 (2016) 1–10, doi: 10.1155/2016/4372136.
- [28] C. Lai, S. Lo, H. Chiang, Adsorption/desorption properties of copper ions on the surface of iron-coated sand using BET and EDAX analyses, *Chemosphere*, 41 (2000) 1249–1255.
- [29] Ç. Üzümlü, T. Shahwan, A.E. Eroğlu, K.R. Hallam, T.B. Scott, I. Lieberwirth, Synthesis and characterization of kaolinite-supported zero-valent iron nanoparticles and their application for the removal of aqueous Cu^{2+} and Co^{2+} ions, *Appl. Clay Sci.*, 43 (2009) 172–181.
- [30] A. Garg, V.K. Sangal, P.K. Bajpai, Decolorization and degradation of Reactive Black 5 dye by photocatalysis: modeling, optimization and kinetic study, *Desal. Water Treat.*, 57 (2016) 18003–18015.
- [31] M. Muruganandham, N. Sobana, M. Swaminathan, Solar assisted photocatalytic and photochemical degradation of Reactive Black 5, *J. Hazard. Mater.*, 137 (2006) 1371–1376.
- [32] C.-L. Hsueh, Y.-H. Huang, C.-C. Wang, C.-Y. Chen, Photoassisted fenton degradation of nonbiodegradable azo-dye (Reactive Black 5) over a novel supported iron oxide catalyst at neutral pH, *J. Mol. Catal. A: Chem.*, 245 (2006) 78–86.
- [33] I.A. Alaton, I.A. Balcioglu, Photochemical and heterogeneous photocatalytic degradation of waste vinylsulphone dyes: a case study with hydrolyzed Reactive Black 5, *J. Photochem. Photobiol., A*, 141 (2001) 247–254.
- [34] I. Arslan, I.A. Balcioglu, T. Tuhkanen, Oxidative treatment of simulated dyehouse effluent by UV and near-UV light assisted Fenton's reagent, *Chemosphere*, 39 (1999) 2767–2783.
- [35] H. Lade, S. Govindwar, D. Paul, Mineralization and detoxification of the carcinogenic azo dye Congo red and real textile effluent by a polyurethane foam immobilized microbial consortium in an upflow column bioreactor, *Int. J. Environ. Res. Public Health*, 12 (2015) 6894–6918.
- [36] A. Rahmani, A. Asadi, A. Fatehizadeh, A.R. Rahmani, M.R. Zare, Interactions of Cd, Cr, Pb, Ni, and Hg in their effects on activated sludge bacteria by using two analytical methods, *Environ. Monit. Assess.*, 191 (2019) 1124–1132, doi: 10.1007/s10661-019-7241-6.
- [37] M.-R. Zare, M.-M. Amin, M. Nikaeen, M. Zare, B. Bina, A. Fatehizadeh, A. Rahmani, M. Ghasemian, Simplification and sensitivity study of Alamar Blue bioassay for toxicity assessment in liquid media, *Desal. Water Treat.*, 57 (2016) 10934–10940.
- [38] M.-R. Zare, M.-M. Amin, M. Nikaeen, B. Bina, A. Rahmani, S. Hemmati-Borji, H. Rahmani, Acute toxicity of Hg, Cd, and Pb towards dominant bacterial strains of sequencing batch reactor (SBR), *Environ. Monit. Assess.*, 187 (2015) 263–270, doi: 10.1007/s10661-015-4457-y.